Monoamine Oxidase A Inhibitor−Near-Infrared Dye Conjugate Reduces Prostate Tumor Growth

Jason Boyang Wu,[†] Tzu-Ping Lin,[‡,§] John D. Gallagher,[‡] Swati Kushal,[‡] Leland W. K. Chung,[†] Haiyen E. Zhau,*,[†] Bogdan Z. Olenyuk,*,[‡,∥] and Jean C. Shih*,[‡,⊥]

[†]Uro-Oncology Research Program, Department of Medicine, Samuel Oschin Comprehensive Cancer Institute, Cedars-Sinai Medical Center, Los Angeles, California 90048, United States

[‡]Department of Pharmacology and Pharmaceutical Sciences, School of Pharmacy, University of Southern California, Los Angeles, California 90089, United States

[⊥]Department of Cell and Neurobiology, Keck School of Medicine, University of Southern California, Los Angeles, California 90033, United States

[∥]USC Norris Comprehensive Cancer Center, Los Angeles, California 90033, United States

S *Supporting Information*

ABSTRACT: Development of anti-cancer agents with high tumor-targeting specificity and efficacy is critical for modern multidisciplinary cancer research. Monoamine oxidase A (MAOA), a mitochondria-bound enzyme, degrades monoamine neurotransmitters and dietary monoamines. Recent evidence suggests a correlation between increased MAOA expression and prostate cancer (PCa) progression with poor outcomes for patients. MAOA induces epithelial−mesenchymal transition (EMT) and augments hypoxic effects by producing excess reactive oxygen species. Thus, development of MAOA inhibitors which selectively target tumors becomes

an important goal in cancer pharmacology. Here we describe the design, synthesis, and *in vitro* and *in vivo* evaluation of **NMI**, a conjugate that combines a near-infrared dye for tumor targeting with the moiety derived from the MAOA inhibitor clorgyline. **NMI** inhibits MAOA with low micromolar IC$_{50}$, suppresses PCa cell proliferation and colony formation, and reduces migration and invasion. In mouse PCa xenografts, **NMI** targets tumors with no detectable accumulation in normal tissues, providing effective reduction of the tumor burden. Analysis of tumor specimens shows reduction in Ki-67^{+} and CD31^{+} cells, suggesting a decrease of cell proliferation and angiogenesis and an increase in M30^{+} cells, indicating increased apoptosis. Gene expression profiles of tumors treated with **NMI** demonstrate reduced expression of oncogenes *FOS*, *JUN*, *NFKB*, and *MYC* and cell cycle regulators *CCND1*, *CCNE1*, and *CDK4/6*, along with increases in the levels of tumor suppressor gene *TP53*, cell cycle inhibitors *CDKN1A* and *CDKN2A*, and MAOA-downstream genes that promote EMT, tumor hypoxia, cancer cell migration, and invasion. These data suggest that **NMI** exerts its effect through tumor-targeted delivery of a MAOA-inactivating group, making **NMI** a valuable anti-tumor agent.
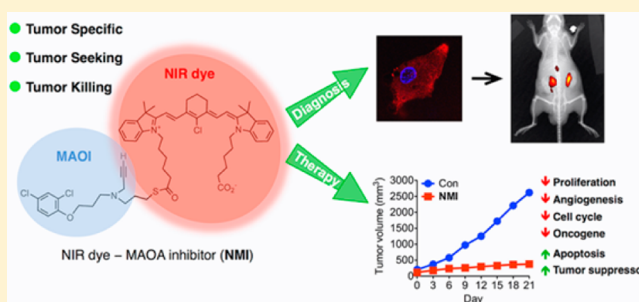
INTRODUCTION

The search for new targets and development of anti-cancer agents with high tumor-targeting specificity and efficacy are critical goals underpinning the urgent, unmet need for more effective, mechanism-based cancer therapies. Monoamine oxidase A (MAOA) is a mitochondria-bound enzyme which catalyzes the degradation of monoamine neurotransmitters and dietary amines by oxidative deamination.[1,2] This process is accompanied by production of hydrogen peroxide, a major source of reactive oxygen species (ROS), which can predispose cancer cells to DNA damage and can be a main cause of tumor initiation and progression.[3,4] Recent studies performed by us[5] and others[6] have shown that increased MAOA levels are associated with prostate cancer (PCa) progression and poor prognosis for patients, and pharmacological inhibition of

MAOA reduces the growth of PCa cells *in vitro* and tumor xenografts *in vivo*.[5,7,8] PCa is the second most common cause of death from cancer in American men of all ages.[9] Despite its widespread occurrence, current treatments that include hormonal therapy,[10] radiation therapy,[11] and surgery[12] are beneficial only for patients in the early stages of the disease and result in undesired side effects. These treatments have limited effectiveness for patients with advanced stages of castration-resistant and metastatic PCa. The urgent, unmet need for novel, effective mechanism-based therapies with reduced side effects has prompted a search for both novel targets in PCa and their pharmacological inhibitors.
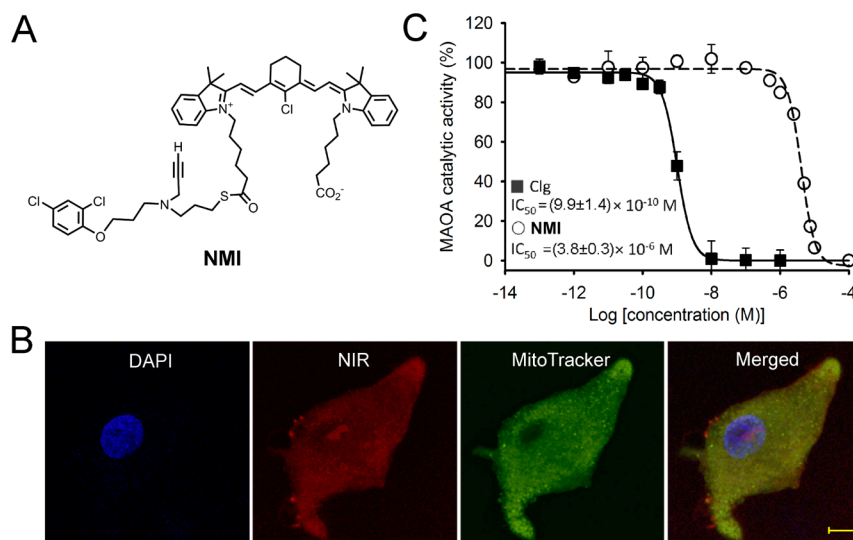
Figure 1. Structure and *in vitro* characterization of **NMI**. (A) Chemical structure of **NMI**. (B) Confocal images of a single LNCaP cell incubated with **NMI**. DAPI and MitoTracker agent were used to stain the nucleus and mitochondria of cells, respectively. Scale bar, 10 μm. (C) Inhibition of MAOA activity was determined in C4-2B cells (see Experimental Section). Clorgyline (Clg) or **NMI** was pre-incubated at 37 °C for 20 min at indicated doses, and IC$_{50}$ values were determined. The assay was performed in triplicate.

Scheme 1. Synthesis of NIR Dye−MAOA Inhibitor Conjugate NMI
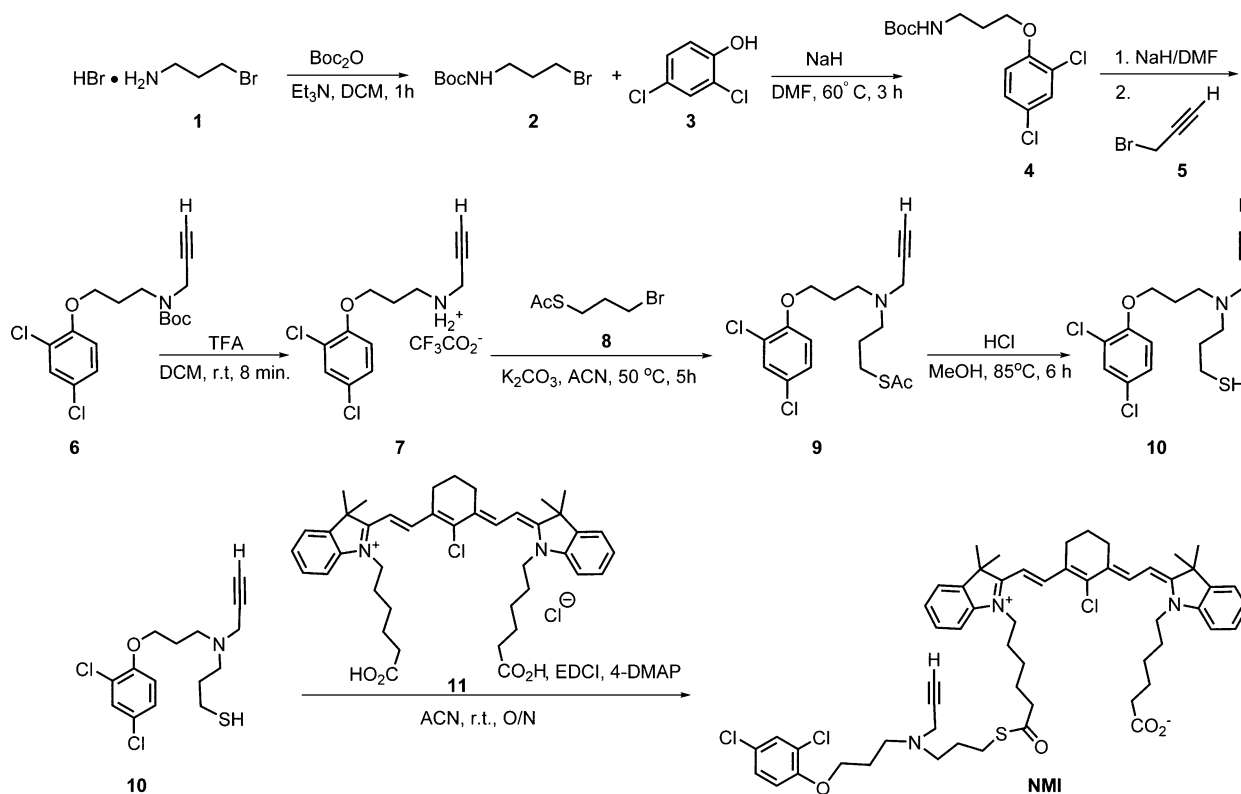
We found that overexpression of MAOA in human PCa cell lines results in a loss of cell polarity, cell−cell adhesion, and gain of migratory and invasive properties, indicating that MAOA induces epithelial−mesenchymal transition (EMT).[5] Moreover, MAOA-dependent activation of oncogenic pathways was consistently detected in high-grade PCa specimens, and knockdown of MAOA reduced or even eliminated prostate tumor growth and metastasis in a variety of PCa xenograft mouse models. By conducting site-directed mutagenesis, we found that MAOA catalytic activity is the major reason for

enhancing growth and metastasis of PCa.[5] MAOA produces hydrogen peroxide as a byproduct of oxidative deamination reactions taking place in the outer membrane of mitochondria. Hydrogen peroxide and products of its conversion as other forms of ROS stabilize hypoxia-inducible factor 1 α (HIF1α).[13−15] HIF1α increases tumor angiogenesis and survival responses as well as invasion and metastasis through the overexpression of hypoxia-inducible genes.[16,17] These results are fully consistent with the clinical data, where elevated
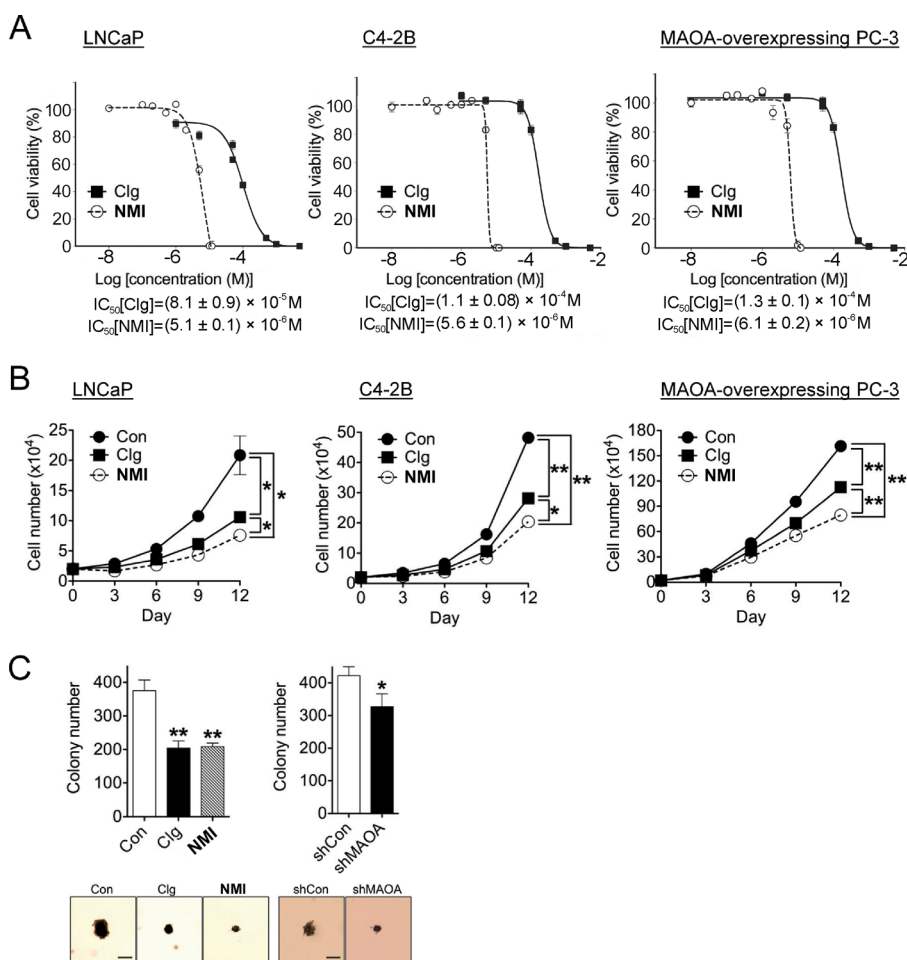
Figure 2. **NMI** inhibits PCa cell proliferation and colony formation. (A) Effect of clorgyline (Clg) and **NMI** on cell viability in LNCaP, C4-2B, and MAOA-overexpressing PC-3 cells as measured by an MTS assay. (B) Cell number counting assay with LNCaP, C4-2B, and MAOA-overexpressing PC-3 cells treated with Clg or **NMI** (1 μM) for 12 days. Compound-added medium was replenished every 3 days; PBS was used as the vehicle. *$p <$ 0.05, **$p <$ 0.01. (C) Colony formation assays in either LNCaP cells treated with Clg or **NMI** (1 μM, left panel) or LNCaP cells targeted by either a scrambled shRNA (shCon) or a MAOA-targeting shRNA (shMAOA). Representative colonies are shown. Original magnification, ×100; scale bar, 50 μm. *$p <$ 0.05, **$p <$ 0.01.

MAOA expression in PCa tissues is correlated with poor prognosis for PCa patients.[5,6]

In keeping with these observations, we investigated MAOA as a potential novel pharmacological target for the treatment of human PCa. MAOA inhibitors, many of which are currently on the market as anti-depressants,[1] target central nervous system and other peripheral tissues where MAOA is present. This reduces the effective systemic concentration of MAOA inhibitors, limiting their delivery into the tumor where they could be most effective. To circumvent these problems, we designed a novel tumor-targeted MAOA inhibitor that would preferentially accumulate in the cancerous lesions. This inhibitor contains a tumor-targeting near-infrared (NIR) dye and a moiety of a MAOA inhibitor. We reasoned that including an NIR imaging functionality could be useful for measuring uptake and cellular localization of the conjugate and possibly for future image-guided diagnosis and drug delivery. We chose the small molecule clorgyline as a MAOA-targeting functionality because of the high affinity and selectivity of this compound toward MAOA. The availability of a high-resolution crystal structure of a clorgyline–MAOA complex[18] facilitated our design. For tumor targeting and NIR imaging, we chose a recently developed class of nontoxic, fluorescent heptamethine

carbocyanine dyes with NIR emission maxima.[19−21] The high selectivity in targeting of these dyes to tumors, mediated by tumor hypoxia and organic anion-transporting polypeptides (OATPs),[22] has been demonstrated for many types of cancers, including human PCa.[23] Here we report the first study on PCa targeting and inhibition of xenograft growth in mice with a designed dual-function NIR dye–MAOA inhibitor conjugate (Figure 1A), abbreviated as **NMI**.

■ RESULTS

Design and Synthesis of NMI. **NMI** was synthesized in a sequence of steps outlined in Scheme 1. The synthesis started with commercially available 3-bromopropylamine hydrobromide (**1**). This compound was converted into *tert*-butyl (3-bromopropyl)carbamate (**2**), which was used in the subsequent step to alkylate the commercially available 2,4-dichlorophenol, giving an intermediate, **4**. Deprotonation of the amide in **4** was carried out with sodium hydride, followed by alkylation with propargyl bromide **5**, producing Boc-protected alkyne **6**. The protecting group was removed under acidic conditions using trifluoroacetic acid (TFA) in dichloromethane (DCM). The product **7** was alkylated with 1-bromo-3-thioacetylpropane (**8**), resulting in the formation of compound

9. Removal of the acetyl protective group in 9 was carried out in methanolic HCl, affording an intermediate, 10. This intermediate was then coupled to MHI-148 dye 11 using 1-ethyl-3-(3-dimethylaminopropyl)carbodiimide (EDCI) and 4-(dimethylamino)pyridine (4-DMAP) to give the product NMI in good yield (Scheme 1). The compound was purified by preparative thin-layer chromatography (TLC), and its identity and purity were confirmed by NMR and mass spectrometry.

NMI Localizes in PCa Cells and Inhibits MAOA. Recent reports suggested that the NIR hepatamethine carbocyanine dyes IR-783 and MHI-148 can be retained in cancer cells but not normal cells, in tumor xenografts, and in spontaneous tumors in transgenic mice.[23] The two dyes have strong emission maxima at 820−860 nm upon excitation at 750−780 nm, which can be easily detected by NIR imaging. MAOA inhibitor−monomethine carbocyanine conjugates have fluorescence properties similar to those of the NIR dye MHI-148 itself. Therefore, a laser-scanning confocal microscope equipped with the appropriate laser and filters for NIR imaging was used to examine the cellular uptake of NMI in human PCa LNCaP cells which have high MAOA levels. Images of a single cell treated with NMI are shown in Figure 1B (*vide supra*). This compound rapidly accumulated in LNCaP cells and localized in the mitochondria, as determined by co-staining with the mitochondria-specific dye MitoTracker Green. In order to test the inhibitory activity of NMI, an MAOA activity assay was carried out in LNCaP-derived C4-2B cells using radiolabeled MAOA-specific substrate serotonin. The results indicate that NMI inhibits MAOA activity with a mean 50% inhibitory concentration (IC_{50}) of $(3.8 \pm 0.3) \times 10^{-6}$ M (Figure 1C).

NMI Reduces Colony Formation, Migration, and Invasion of PCa Cells. PCa LNCaP, C4-2B and MAOA-overexpressing PC-3 cells[5] were used for cell viability (Figure 2A) and cell proliferation assays (Figure 2B). Treatment with clorgyline produced dose−response curves with $IC_{50} = 80.7 \pm 8.8$ μM in LNCaP, 113.5 ± 8.0 μM in C4-2B, and 129.3 ± 9.6 μM in MAOA-overexpressing PC-3 cells. By comparison, treatment with NMI produced curves with $IC_{50} = 5.1 \pm 0.1$ μM in LNCaP, 5.6 ± 0.1 μM in C4-2B, and 6.1 ± 0.2 μM in MAOA-overexpressing PC-3 cells, indicating 12−20 times higher efficacy for NMI in inhibiting PCa cells growth as compared to clorgyline (Figure 2A).

Most PCa cell lines, including LNCaP, C4-2B, and MAOA-overexpressing PC-3, possess undetectably low levels of monoamine oxidase B (MAOB), the second known MAO isoform.[24] However, given the important role MAOB plays in the normal physiology of the central nervous system and peripheral tissues,[2] we first decided to ascertain that MAOA is selectively inhibited with minimal interference to MAOB. Given that clorgyline is selective for MAOA and produces dose-sensitive inhibition,[2] in our preliminary cell-based assays we used a range of clorgyline concentrations (10 nM−10 μM) that are inhibitory for MAOA but below the IC_{50} for MAOB inhibition.[25] We determined 1 μM as the lowest concentration required for clorgyline to show efficacy in suppressing cell proliferation. This concentration was also consistent with the data from other reported study.[24] Thus, we chose 1 μM as the concentration at which the efficacies of both clorgyline and NMI could be assessed and compared in the subsequent *in vitro* studies.

In cell number counting assays, we observed that both clorgyline and NMI reduced the number of proliferating cells after 12 days. NMI also showed higher efficacy as compared to

clorgyline (Figure 2B). Colony formation assays were performed in LNCaP cells treated with clorgyline or NMI (Figure 2C). In a parallel setup, LNCaP cells were targeted by either MAOA-targeting shRNA (shMAOA) or a scrambled shRNA (shCon). Treatment with clorgyline and NMI resulted in a reduction of the colony number by as much as 45%, although in this assay the difference between the activities of clorgyline and NMI was not statistically significant (Figure 2C, left panel). Treatment with MAOA-targeting shRNA reduced the colony number by only 25%, as compared to treatment with scrambled shRNA (right panel). Because clorgyline has consistently shown lower efficacy in these experiments, we focused on NMI in the subsequent studies.

We tested the ability of NMI to inhibit migration of LNCaP and C4-2B cells. After treatment with compounds at 1 μM concentration for 48 h, the LNCaP cells showed statistically significant reduction in migration of 35% for NMI (Figure 3A,
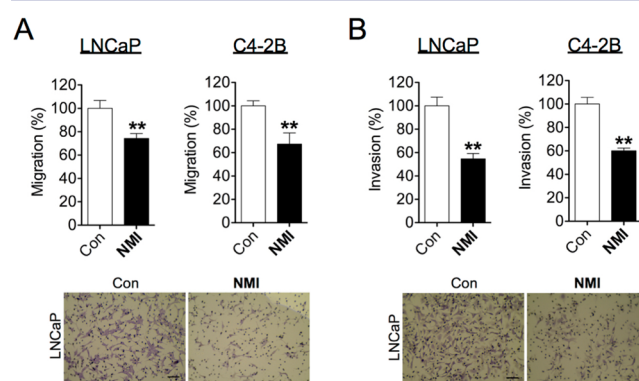

Figure 3. NMI reduces the migration and invasion of PCa cells. (A) Migration assays and (B) invasion assays of LNCaP and C4-2B cells treated with NMI (1 μM, 48 h). Representative images from LNCaP cells are shown. Original magnification, ×200; scale bars, 200 μm. **$p < 0.01$.

left panel). A similar result was observed for C4-2B cells (Figure 3A, right panel). In invasion assays, cells treated with NMI also showed 50% reduction in LNCaP and 40−45% reduction in C4-2B cells (Figure 3B).

NMI Reduces the Rate of Growth of PCa Xenografts in Nude Mice. In order to assess the efficacy of NMI *in vivo*, subcutaneous tumor xenograft mouse models were used. After being implanted subcutaneously into male nude mice, C4-2B cells formed tumors in 3−4 weeks. After tumors reached 200 mm³, mice were randomly assigned into two groups to receive treatments every other day: (1) control and (2) NMI. Two routes of administration were used to test the tumor-specific targeting ability of NMI: intratumoral and intraperitoneal. Tumors were measured with calipers, and tumor volume was calculated every 3 days during the 21-day treatment. Serum prostate-specific antigen (PSA) levels in mice were determined on day 11 (the middle of the treatment course), and tumor MAOA activity was determined at the end of treatment. Mice body weights were monitored on a weekly basis from the time of inoculation. At the experiment end point, mice were euthanized, tumors were excised, and tumor weights were determined. NMI-treated mice showed significant delays in tumor growth (Figure 4A), reduction in PSA levels (Figure 4B), and decreases in tumor weight as compared to control mice (Figure 4C). NIR imaging of the whole body *in vivo* and individual tumor and normal organs *ex vivo* clearly showed
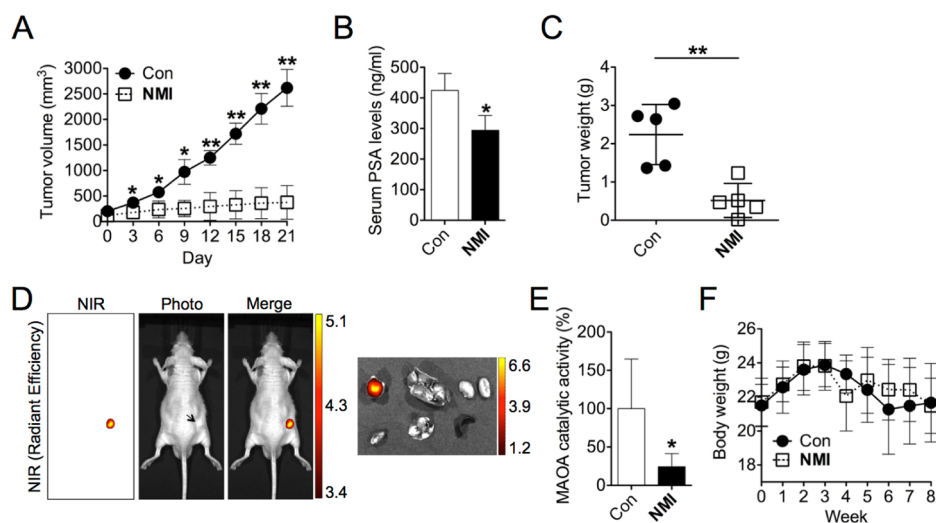
Figure 4. **NMI** inhibits the growth of C4-2B tumor xenografts in mice. (A) C4-2B cells were subcutaneously injected into male nude mice ($n = 5$ for each group) to establish tumor xenografts. After tumor size reached 200 mm^3, mice were given intratumoral treatments (saline and **NMI**; 750 nmol/mouse) every other day for a 21-day period. Tumor size was determined by calipers, and tumor volume was calculated as described in the Supporting Information. *$p < 0.05$, **$p < 0.01$. (B) Serum PSA levels in mice were determined on day 11 after the treatment by ELISA. *$p < 0.05$. (C) Tumor weight, determined at the time of euthanasia of mice. **$p < 0.01$. (D) *In vivo* and *ex vivo* NIR imaging of mice given **NMI** treatment. Representative images are shown. NIR fluorescence color scales denote ×10^9 and ×10^8 for *in vivo* and *ex vivo* imaging, respectively, in the units of radiant efficiency ([p/sec/cm^2/sr]/[μW/cm^2]). (E) Tumor MAOA catalytic activity, determined at the time of euthanasia. *$p < 0.05$. (F) Mice body weight, determined every week after tumor implantation.

NMI localization within the tumor (Figure 4D). Measurements of MAOA activity in tumors showed its significant reduction in **NMI**-treated mice (Figure 4E). All mice in treated and control groups showed similar changes in body weight that did not exceed 18% throughout the entire duration of experiment (Figure 4F), suggesting that this treatment regimen was well tolerated by the animals.

We next performed hematoxylin and eosin (H&E) staining and immunohistochemical analysis of protein expression patterns of Ki-67 (a cell proliferation marker), M30 (a cell apoptosis marker), and CD31 (an angiogenesis marker) in tumor specimens from control and treated groups (Figure 5A). H&E staining showed a decrease in the nucleus-to-cytoplasm ratios in cells from tumors treated by **NMI** as compared to the control group, suggesting reduced malignancy in treated tumors.[26] Ki-67 staining of tumor specimens revealed a 25% decrease of Ki-67$^+$ cells in **NMI**-treated tumors (Figure 5B, left panel). We observed an 11-fold increase of M30$^+$ area (middle panel) and a 48% decrease in CD31$^+$ area (right panel) in the treated specimens as compared to controls (Figure 5B), suggesting increased apoptosis and reduced angiogenesis occurring in treated tumors.

Gene expression profiling further indicated down-regulation in expression of such proto-oncogenes or oncogenes as *FOS*, *JUN*, *NFKB1*, and *MYC* and up-regulation of *TP53* tumor suppressor gene expression in response to treatment. Cell-cycle regulator genes that activate cell cycle progression, such as *CCND1*, *CCNE1*, *CDK4*, and *CDK6*, were also down-regulated, whereas expression of select cell-cycle inhibitors, including *CDKN1A* and *CDKN2A*, increased in the **NMI**-treated tumors as compared to controls. In contrast, decreased expression of anti-apoptotic *BCL2* gene was revealed in treated tumor samples. In addition, genes involved in MAOA-downstream signaling demonstrated to promote EMT (*VIM*, *SNAI1*, *SNAI2*, and *TWIST1*), tumor hypoxia (*VEGFA* and *GLUT1*), and cancer cell migration, invasion, and metastasis (*IL6*, *IL8*,

MMP2, *MMP9*, and *MET*)[5] all showed reduced expression by treatment (Figure 5C).

To further evaluate the tumor-targeting properties of **NMI**, C4-2B cells were subcutaneously implanted contralaterally into both flanks of male nude mice. After the formation of two tumor xenografts in each mouse, **NMI** was injected intratumorally into one of the lesions. NIR imaging conducted after three injections performed every other day showed localization of the conjugate in both tumors (Figure 6A), which reveals tumor-targeting properties of **NMI**. Remarkably, the intensities of the NIR signals originating from the injected and contralateral tumor were comparable, suggesting rapid redistribution of the injected compound between two tumors. Figure 6B further shows that **NMI** selectively targets two tumors when administered in an intraperitoneal injection. NIR imaging shows no observable NIR signals in other body parts, further confirming the tumor-specific targeting of **NMI** and its systemic circulation.

■ DISCUSSION

The search for effective therapies based on pharmacological targeting and inhibition of increased MAOA expression in PCa and potentially other cancers is in its infancy. This study is our first report on the design, synthesis, and *in vitro* and *in vivo* evaluation of the therapeutic efficacy of **NMI**, a novel conjugate that targets tumors and reduces MAOA activity in mouse PCa xenograft models. The conjugate consists of the MAOA targeting functionality and a NIR dye. It was synthesized in eight steps in a scalable procedure from commercially available starting materials to give hundreds of milligrams of material. The conjugate was shown to target PCa cells, localize in mitochondria, and inhibit MAOA activity in the low micro-molar IC$_{50}$ range. It has shown efficacy that exceeds that of clorgyline, a known MAOA inhibitor, in suppressing the growth of three PCa cell lines with high levels of MAOA: LNCaP, C4-2B, and MAOA-overexpressing PC-3. It inhibited colony
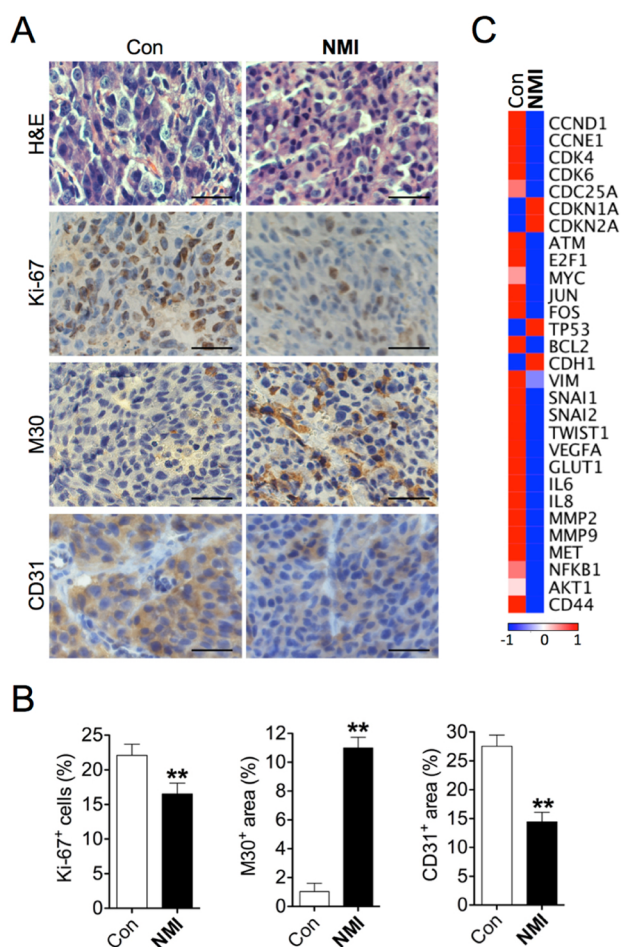
A

B

C

Figure 5. Analysis of tumor specimens obtained from treated and control mice. (A) H&E and immunohistochemical analysis of Ki-67, M30, and CD31 expression in respective tumor specimens. Representative images are shown. Original magnification, ×400; scale bars, 20 μm. (B) Quantification of percent of Ki-67^{+}, M30^{+}, and CD31^{+} tumor cells or areas of five distinct images from each group. The data represent mean ± SD. **$p < 0.01$. (C) Heat map depicting gene expression profiling of tumor samples from each group. Red and blue colors indicate high and low relative expression levels, respectively, with the numbers indicating log$_2$-transformed ratios.

formation for LNCaP cells similarly to MAOA-targeting shRNA. **NMI** also inhibited invasion and migration of PCa cells, which is consistent with the demonstrated mechanism that high MAOA activity is associated with aggressive cell behavior and induced EMT. The diminished levels of an epithelial marker, E-cadherin, and increased expression of a mesenchymal marker, vimentin, indicate EMT suppression. By conducting a comparative study using **NMI** and clorgyline, we have shown that the tumor-targeting property of **NMI** makes it a superior pharmacological inhibitor, as compared to clorgyline, in nearly all cases.

Our *in vivo* studies using PCa xenograft mouse models show that **NMI** localizes in the tumors, reduces the rate of tumor growth, and decreases levels of PSA and MAOA catalytic activity in mice engrafted with C4-2B cells. At a final dose of 6 nmol per mouse, **NMI** shows significant inhibitory efficacy on tumor xenograft growth. One of the unexpected findings is the discovery that an intratumorally injected compound would redistribute itself into the neighboring tumors, suggesting that its redistribution *in vivo* is facilitated by the rapid circulation in

the bloodstream. This is further supported by the observation of tumor-specific targeting made by an intraperitoneal administration.

We previously shown that tumor hypoxia is one of the major factors that mediates uptake of heptamethine carbocyanine NIR dyes by tumor cells.[22] Hypoxia, through stabilization of HIF1α, also underlies one of the key MAOA functions in promoting tumor progression and metastasis in PCa.[5] The increased uptake and retention of **NMI** in tumors is likely due to tumor hypoxia through an activated HIF1α/OATPs signaling axis,[22] which is supported by our observation that the tumor-targeting effect of **NMI** could be enhanced in PCa expressing high levels of MAOA associated with increased tumor hypoxia. Indeed, the higher accumulation of **NMI** in MAOA-overexpressing PC-3 tumors as compared to a control tumor is paralleled by the increase in HIF1α immunostaining in those tumor samples with elevated expression of MAOA (see Supporting Information, Figure S1). These observations suggest that a synergistic strategy based on the use of tumor-targeting MAOA inhibitors such as **NMI** and inhibitors of hypoxia-inducible transcription could result in an improved efficacy and reduced side effects in treating hypoxic, high-grade PCa.

■ CONCLUSION

We have demonstrated that a tumor-targeting NIR dye—MAOA inhibitor conjugate has the highest efficacy among all the MAOA inhibitors tested in PCa, and it may become a novel pharmacological agent for treatment and diagnosis of this type of cancer. Such an agent, after the proper preclinical development, could become an important platform for future generation of anti-cancer therapeutics. Such a conjugate also possesses a diagnostic potential, in that it can differentiate the prostate tumors with high MAOA activity, high hypoxia, and elevated malignant potential from the indolent neoplasms. Its anti-tumor effect, largely derived through MAOA targeting, makes it a valuable addition to the anti-cancer therapeutic armamentarium.

■ EXPERIMENTAL SECTION

General. All reagents and solvents were obtained from commercial sources and were used as received unless otherwise stated. Molecular biology grade salts and buffers were obtained from Sigma-Aldrich. MitoTracker Green and 4′,6-diamidino-2-phenylindole (DAPI) dyes were obtained from Life Technologies. All reactions involving moisture-sensitive reagents were conducted under argon atmosphere with anhydrous solvents and flame-dried glassware. Hygroscopic liquids were transferred via a syringe and were introduced into reaction vessels through rubber septa. Reaction product solutions were concentrated using a rotary evaporator at 30−150 mmHg. Column chromatography was performed on silica gel (230−400 mesh) using reagent grade solvents. Analytical TLC was performed on glass-backed, pre-coated plates (0.25 mm, silica gel 60, F-254, EM Science). Analytical high-performance liquid chromatography (HPLC) was performed on Microsorb-MV C$_8$ reverse-phase columns (250 × 4.6 mm, Varian) using a Shimadzu LC-10A VP pump and a Shimadzu SPD 10A VP UV−vis variable-wavelength detector. Preparative HPLC purifications were carried out with C$_8$ reverse-phase preparative columns (Grace Davison). The flow rate for preparative reverse-phase HPLC was 4 mL/min. In all cases, 5%−95% gradients of acetonitrile (ACN) in 0.1% aqueous TFA were used as eluents. Water (18 MΩ) was obtained from a Barnstead water purification system, and all buffers were 0.2 μm filtered. NMR spectra were collected on instruments in the indicated solvents. The identity and purity of each intermediate and the final product were confirmed by ^{1}H and [13]C
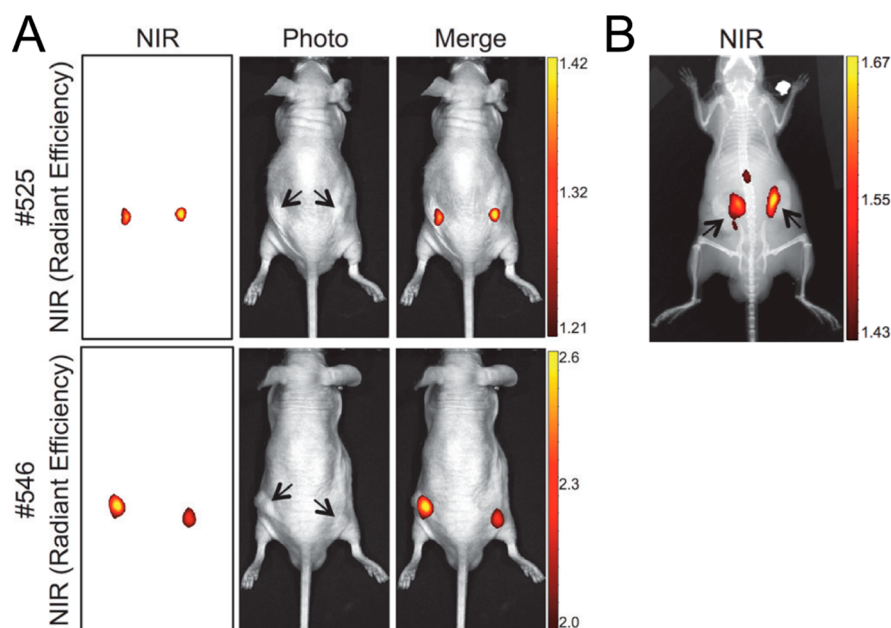
Figure 6. Tumor-targeting properties of **NMI** in mouse xenografts. (A) C4-2B cells were subcutaneously implanted into both flanks of male nude mice to form tumor xenografts, and only the tumor in one flank (right #525 or left #546) was given intratumoral injection of **NMI** (12 nmol/mouse) every other day for three injections, followed by NIR imaging. Representative images are shown. (B) Mice bearing C4-2B tumor xenografts as described in (A) were intraperitoneally injected with **NMI** (50 nmol/mouse) and 24 h later subjected to NIR imaging. One representative image is shown. Tumors are indicated by the arrows. NIR fluorescence color scales denote ×10^9 and ×10^{10} for intratumoral and intraperitoneal injections, respectively, in the units of radiant efficiency ([p/sec/cm^2/sr]/[μW/cm^2]).

NMR (Varian Mercury 400 MHz instrument) and mass spectrometry (Agilent 6520 time-of-flight system).

Synthesis of Compounds. *tert-Butyl (3-Bromopropyl)-carbamate (2).* To a 100 mL round-bottom flask equipped with a magnetic stirrer were added 3-bromopropylamine hydrobromide (**1**, 1.19 g, 5.44 mmol, 1.0 equiv) and DCM (30 mL). To the resultant solution was added di-*tert*-butyl dicarbonate (2.16 g, 9.90 mmol, 1.8 equiv) in DCM (20 mL), followed by triethylamine (0.866 mL, 6.21 mmol, 1.1 equiv). The solution was stirred at room temperature for 75 min. The reaction was diluted with DCM (50 mL) and washed twice with sodium bicarbonate (50 mL) and once with brine (50 mL). The organic phase was dried over sodium sulfate and filtered, and the solvent was removed *in vacuo* to yield **2** (1.35 g, 80%). ^{1}H NMR (400 MHz, CDCl$_3$): δ 4.65 (s, 1H), 3.37 (dt, 2H, J_1 = 6.4 Hz, J_2 = 1.2 Hz), 3.21 (dd, 2H, J_1 = 12.4 Hz, J_2 = 6.4 Hz), 1.98 (m, 2H), 1.37 (s, 9H).

tert-Butyl 3-(2,4-Dichlorophenoxy)propylcarbamate (4). To a 50 mL round-bottom flask equipped with a magnetic stirrer was added 2,4-dichlorophenol (**3**, 452 mg, 2.77 mmol, 1.0 equiv) followed by dimethylformamide (DMF, 3 mL). To the resultant solution was added sodium hydride portion-wise (111 mg, 2.77 mmol, 1.0 equiv) followed by **4** (661 mg, 2.77 mmol, 1.0 equiv) in DMF (2 mL). The mixture was stirred at 60 °C for 3 h. The reaction was diluted with DCM (50 mL) and washed three times with 10% sodium hydroxide (15 mL), once with HCl (25 mL), and once with brine (50 mL). The organic phase was dried over sodium sulfate and filtered, and the solvent was removed *in vacuo* to yield **4** (431 mg, 48%). ^{1}H NMR (400 MHz, CDCl$_3$): δ 7.36 (d, 1H, J = 2.8 Hz), 7.18 (dd, 1H, J_1 = 8.8 Hz, J_2 = 2.8 Hz), 6.83 (d, 1H, J = 8.4 Hz), 5.16 (s, 1H), 4.07 (t, 2H, J = 5.6 Hz), 3.38 (m, 2H), 2.03 (m, 2H), 1.44 (s, 9H).

tert-Butyl 3-(2,4-Dichlorophenoxy)propyl(prop-2-ynyl)carbamate (6). To a 20 mL scintillation flask equipped with a magnetic stirrer was added **4** (273 mg, 0.858 mmol, 1.0 equiv) followed by DMF (3 mL). To the resultant solution was added sodium hydride portion-wise (35 mg, 0.858 mmol, 1.0 equiv) followed by propargyl bromide (**5**, 130 μL, 0.858 mmol, 1.0 equiv). The mixture was stirred at room temperature for 2 h. The reaction was evaporated and the residue purified by column chromatography using a gradient of 2%−5%−50% EtOAC in hexanes to yield **6** (75.4 mg, 21% yield). ^{1}H NMR (400

MHz, CDCl$_3$): δ 7.36 (d, 1H, J = 2.8 Hz), 7.17 (dd, 1H, J_1 = 8.4 Hz, J_2 = 2.4 Hz), 6.83 (d, 1H, J = 8.8 Hz), 4.07 (t, 2H, J = 6.0 Hz), 4.04 (t, 1H, J = 5.6 Hz), 3.56 (t, 2H, J = 6.8 Hz), 2.18 (t, 2H, J = 2.4 Hz), 2.03 (m, 2H), 1.57 (s, 2H), 1.44 (s, 9H).

N-(3-(2,4-Dichlorophenoxy)propyl)prop-2-yn-1-aminium Trifluoroacetate (7). To a 20 mL scintillation flask equipped with a magnetic stirrer was added **6** (72.6 mg, 0.858 mmol, 1.0 equiv) followed by DCM (4 mL). To the resultant solution was added TFA (1 mL). The mixture was stirred at room temperature for 8 min. The reaction was evaporated and dried *in vacuo* to provide **7** without further purification (75 mg, quantitative yield).

S-3-Bromopropyl Ethanethioate (8). A 250 mL three-neck round-bottom flask equipped with a thermocouple in a glass sleeve, a magnetic stirrer, a vigreux column with an argon inlet (middle stem), and a sleeved rubber septum stopper was assembled and dried with a heat gun under flow of argon. Approximately 110−120 mL of anhydrous DMF was added via a cannula. Potassium thioacetate (11.68 g, 102.3 mmol) was added portion-wise into the flask while it was cooled with an ice-cold MeOH bath. The reaction was stirred for 7 h at about −10 °C. The ice-cold MeOH bath was removed after the reaction was quenched by addition of 165 mL of water. The reaction mixture was partitioned with 300 mL of methyl *tert*-butyl ether (MTBE) and 700 mL of water. The water layer was washed with 200 mL of MTBE. The MTBE layers were washed sequentially with water, saline, and NaHCO$_3$, dried over MgSO$_4$, filtered, and evaporated to yield **8** (19.1 g, 98.7%). ^{1}H NMR (400 MHz, CDCl$_3$): δ 3.45 (t, 2H, J = 6.4 Hz), 3.01 (t, 2H, J = 7.2 Hz), 2.35 (s, 3H), 5.16 (s, 1H), 2.13 (m, 2H).

S-3-((3-(2,4-Dichlorophenoxy)propyl)(prop-2-ynyl)amino)propyl Ethanethioate (9). To a 20 mL scintillation vial equipped with a magnetic stirrer was added **7** (12 mg, 0.032 mmol, 1.0 equiv) followed by ACN (2.5 mL). To the resultant solution was added potassium carbonate (186 mg, 1.343 mmol, 10.0 equiv) followed by **8** (12.6 mg, 5.66 mmol, 17.7 equiv). The mixture was stirred at 80 °C overnight. The reaction was then filtered, the solvent was removed under reduced pressure, and the residue was dried *in vacuo*. The crude material was purified by preparative TLC using 5% ethyl acetate in hexanes as an eluent to yield **9** (4.7 mg, 39%). ^{1}H NMR (400 MHz, CDCl$_3$): δ 7.35

(d, 1H, J = 2.4 Hz), 7.16 (dd, 1H, J = 8.4 Hz, J = 2.4 Hz), 7.35 (d, 1H, J = 8.8 Hz), 4.07 (t, 2H, J = 6.0 Hz), 4.04 (t, 1H, J = 5.6 Hz), 3.40 (s, 2H), 2.87 (t, 2H, J = 6.8 Hz), 2.70 (t, 2H, J = 6.4 Hz), 2.56 (t, 2H, J = 6.8 Hz), 2.30 (m, 3H), 2.17 (s, 1H), 1.95 (m, 2H), 1.71 (m, 2H).

*3-((3-(2,4-Dichlorophenoxy)propyl)(prop-2-ynyl)amino)propane-1-thiol (**10**).* A solution of **9** (1.17 mg, 3.10 μmol) in 200 μL of ACN was added into a 20 mL vial equipped with a stir bar, evaporated, and then co-evaporated with MeOH three times to remove ACN. MeOH/HCl (200 μL) was added into the vial, and then the vial was heated on an oil bath at 85 °C for 6 h. The reaction mixture was co-evaporated sequentially with MeOH three times and ACN three times to give **10**, which was used in the next step without further purification.

*6-((Z)-2-((E)-2-(2-Chloro-3-((E)-2-(1-(6-((3-((3-(2,4-dichlorophenoxy)propyl)(prop-2-yn-1-yl)amino)propyl)thio)-6-oxo-hexyl)-3,3-dimethyl-3H-indol-1-ium-2-yl)vinyl)cyclohex-2-en-1-ylidene)ethylidene)-3,3-dimethylindolin-1-yl)hexanoate (**NMI**).* MHI-148 **11** (170 mg, 242 μmol, 1.10 equiv), dry DCM (10 mL), EDCI hydrochloride (45 mg, 235 μmol, 1.04 equiv), and DMAP (8 mg, 6.5 μmol, 0.03 equiv) were added to a 20 mL round-bottom flask equipped with a stir bar and stirred for 15 min. Compound **10**, obtained in the previous step (75 mg, 226 μmol, 1.00 equiv), was added to the mixture as a solution in ACN (2 mL), and the reaction was stirred at room temperature overnight. The solvent was then removed under reduced pressure. The compound was dissolved in 5 mL of DCM and purified on preparative silica gel plates using 7.5% MeOH in DCM as an eluent. Yield: 83.2 mg, 37%. Alternatively, the reaction mixture aliquot was dissolved in methanol and purified by HPLC using a YMC HPLC column (C_{18} 5-μm column, 50 mm length ×20 mm i.d.) and a 5%−95% gradient of ACN in 0.1% aqueous TFA over 30 min to yield **NMI** (0.144 mg recovery). ^{1}H NMR (400 MHz, CDCl$_3$): δ 1.49 (m, 2H, γ-CH$_2$(COOH)), 1.56 (m, 2H, γ-CH$_2$(COSCH$_2$−)), 1.67 (s, 6H, CH$_3$), 1.71 (s, 6H, CH$_3$), 1.80 (m, 2H, β-CH$_2$), 1.82 (m, 2H, β-CH$_2$), 1.86 (m, 2H, δ-CH$_2$), 1.88 (m, 2H, δ-CH$_2$), 1.94 (s, 2H, O-CH$_2$CH$_2$CH$_2$N−), 1.97 (s, 2H, S-CH$_2$CH$_2$CH$_2$N−), 2.09 (s, 2H, CH$_2$), 2.56−2.57 (m, 4H, α-CH$_2$), 2.68−2.70 (m, 4H, CH$_2$NCH$_2$), 2.71 (s, 2H, CH$_2$C=), 2.75 (s, 2H, CH$_2$C=), 2.85 (m, 2H, −SCH$_2$), 4.04 (t, 1H, HC≡C−), 4.05 (t, 4H, N−CH$_2$), 4.05 (t, 2H, O−CH$_2$), 4.07 (t, 2H, CH$_2$C≡), 6.04 (d, 1H, CH=CH), 6.32 (d, 1H, CH=CH), 6.85 (d, 1H, Ar-H), 7.05 (d, 1H, Ar-H), 7.17−7.42 (m, 9H, Ar-H), 8.28 (d, 1H, CH=CH), 8.40 (d, 1H, CH=CH). HRMS: calcd for C$_{57}$H$_{69}$Cl$_3$N$_3$O$_4$S m/z 996.4074; observed m/z 996.4068. λ_{max} absorption and fluorescence wavelengths in methanol were 780 and 802 nm, respectively.

Cell Lines and Cell Culture Conditions. Human PCa LNCaP cell line was obtained from American Type Culture Collection. Human PCa C4-2B cell line was established from LNCaP as described previously.[27] Human PCa MAOA-overexpressing PC-3 cell line was established as described previously.[5] LNCaP and C4-2B cells were grown in RPMI 1640 medium (Life Technologies), and MAOA-overexpressing PC-3 cells were grown in T-medium (Life Technologies), with both media supplemented with 10% fetal bovine serum (FBS) and 1% penicillin/streptomycin.

Laser-Scanning Confocal Microscopy. Cells were plated in glass-bottom microscopy dishes (MatTek) at a density of 20 000 cells in 400 μL of medium supplemented with 10% FBS and were allowed to form a monolayer over 20 h. **NMI** at a concentration of 5 μM in 400 μL of fresh medium containing 10% FBS, MitoTracker Green (1×), and DAPI (1×) were added to the media, and the cells were incubated at 37 °C and 5% CO$_2$ for an additional 4 h. Imaging was performed on a Zeiss LSM 510 inverted laser-scanning confocal microscope, equipped with an oil-immersion ×63 objective lens. Excitation wavelengths were set at λ_{max} = 488 nm (DAPI, blue excitation), 514 nm (MitoTracker Green, green-yellow excitation), and 790 nm (**NMI**, red excitation). The data were acquired in a multi-track mode. Images were taken using pinholes of 130−200 μm in order to capture fluorescence signals on a thin focus plane.

MAOA Catalytic Activity Assay. MAOA catalytic activity was determined in PCa cells and tumor samples treated with clorgyline or **NMI** at different concentrations. One hundred micrograms of total protein (~1 × 10^6 cells) were incubated with 1 mM ^{14}C-5-hydroxytryptamine (5-HT) in the assay buffer (50 mM sodium phosphate buffer, pH 7.4) at 37 °C for 20 min, and the reaction was terminated by the addition of 100 μL of 6 N HCl. The reaction products were extracted with benzene/ethyl acetate and centrifuged. The organic phase containing the reaction products was extracted, and the radioactivity was determined by liquid scintillation spectroscopy.

Cell Proliferation Assays. Cells were seeded on 96-well plates in triplicate and treated with vehicle, clorgyline, or **NMI** at different concentrations for 96 h. Cell proliferation was determined by MTS assay (Promega) following the manufacturer's instructions. For cell number counting assays, cells were seeded on 6-well plates (2 × 10^4 cells/well) and treated with vehicle, clorgyline (1 μM), or **NMI** (1 μM) for 12 days, with compound-added medium replenished every 3 days. Cell numbers from triplicate wells were counted by a hemocytometer.

Colony Formation Assay. Cells were suspended in the culture media containing 0.3% agarose (FMC BioProducts) with vehicle, clorgyline (1 μM), or **NMI** (1 μM) and placed on top of solidified 0.6% agarose in 6-well plates. The developed colonies were counted and recorded under a microscope after a 3-week incubation.

Migration and Invasion Assays. Assays were performed using 6.5 mm transwells (8 μm pore size) coated with either collagen I or Growth Factor Reduced Matrigel (BD Biosciences) for the migration and invasion assays, respectively. Cells were serum-starved overnight before seeding to eliminate the interference of proliferative effect with cell migration or invasion. Cells were seeded inside transwell inserts containing culture medium without serum and with treatment. After 18−24 h, the cells that translocated to the lower surface of the filters were fixed in 4% formaldehyde. The fixed membranes were stained using crystal violet (1% solution). Assays were quantified by counting the number of stained nuclei in five independent fields in each transwell.

Mouse Subcutaneous Tumor Xenograft Studies. Male 4- to 6-week-old athymic nude mice were purchased from Taconic, Inc., housed in the animal research facility at University of Southern California (USC), and fed a normal diet. For xenograft studies, 2 × 10^6 C4-2B cells were mixed 1:1 with Matrigel (BD Biosciences) and injected subcutaneously into nude mice, with each mouse bearing one tumor on the right flank. After tumors reached a size of 100−200 mm^3, mice were randomly assigned to two groups (saline or **NMI**, n = 5 per group). For the treatment group, intratumoral injections of **NMI** (2 μg/tumor, 250 nmol/mouse) were given to mice every other day for the first 10 days, and then the dose was increased to 6 μg/tumor (750 nmol/mouse). Intratumoral injections of saline were given to the control group. Tumor size was measured every 3 days by calipers, and tumor volume was calculated by the formula of length × width^2 × 0.52.[28] Mouse blood was collected from the retro-orbital sinus bleeding on day 11, and serum PSA level was determined by an ELISA kit (GenWay Biotech) in accordance with the manufacturer's instructions. Tumors were dissected and weighed when mice were euthanized on day 21. Mice body weight was measured on a weekly basis following tumor implantation. All animal studies received prior approval by the USC IACUC and were conducted in compliance with its recommendations.

Analysis of Tumor Uptake of NMI by NIR Fluorescence Optical Imaging. Mice bearing C4-2B subcutaneous tumors, when tumor size reached 2−6 mm in diameter assessed by palpation, were injected intratumorally (three consecutive injections every other day) with **NMI** at a dose of 12 nmol/mouse or intraperitoneally (one injection) at 50 nmol/mouse. Whole-body NIR fluorescence optical imaging was taken 24 h after the last injection using an IVIS Lumina XR imaging system (PerkinElmer) equipped with fluorescence filter sets (excitation/emission, 783/840 nm) as described previously.[29] During imaging, mice were maintained in an anesthetized state.

Immunohistochemistry. Immunohistochemical analysis of tumor xenograft samples was performed using antibodies against Ki-67 (Abcam), M30 (DiaPharma), or CD31 (Santa Cruz) following our published protocol[30] with minor modifications. Briefly, formalin-fixed paraffin-embedded sections (4 μm) were de-paraffinized, rehydrated, and subjected to antigen retrieval. After incubation in Dual

Endogenous Enzyme Block solution (Dako) for 10 min, the section was treated with primary antibody diluted by different folds with Antibody Diluent solution (Dako) at 4 °C overnight. The section was then washed three times in phosphate-buffered saline containing 0.2% Tween-20 for 5 min per washing. To detect specific staining, the section was treated for 30 min with EnVision + Dual Link System-HRP (Dako), which contained horseradish peroxidase-conjugated goat antibodies against mouse or rabbit IgG. The section was washed three times for 5 min each, and specific stains were developed with 3,3-diaminobenzidine (Dako). Images were acquired using a Nikon camera and software. Magnification was ×400 (scale bars ∼20 μm). Percent of Ki-67$^+$ cells and M30$^+$ and CD31$^+$ area were analyzed by ImageJ software (NIH).

Statistical Analysis. Data are presented as the mean ± SD, as indicated in the figure legends. All comparisons were analyzed by unpaired two-tailed Student's t-test. A p-value less than 0.05 was considered to be statistically significant.

■ ASSOCIATED CONTENT

Ⓢ Supporting Information

Figure S1, detailed description of reverse transcription and quantitative real-time PCR assays, and Table S1. This material is available free of charge via the Internet at http://pubs.acs.org.

■ AUTHOR INFORMATION

Corresponding Authors
*jcshih@usc.edu
*bogdan@usc.edu
*haiyen.zhau@cshs.org

Present Address
§T.-P.L.: Department of Urology, Taipei Veterans General Hospital, Taipei, Taiwan 11217, R.O.C., and Department of Urology, School of Medicine, and Shu-Tien Urological Research Center, National Yang-Ming University, Taipei, Taiwan 11217, R.O.C.

Notes
The authors declare no competing financial interest.

■ ACKNOWLEDGMENTS

■ REFERENCES

(1) Bortolato, M.; Chen, K.; Shih, J. C. *Adv. Drug Delivery Rev.* **2008**, *60*, 1527.

(2) Shih, J. C.; Chen, K.; Ridd, M. J. *Annu. Rev. Neurosci.* **1999**, *22*, 197.

(3) Josson, S.; Nomura, T.; Lin, J. T.; Huang, W. C.; Wu, D.; Zhau, H. E.; Zayzafoon, M.; Weizmann, M. N.; Gururajan, M.; Chung, L. W. *Cancer Res.* **2011**, *71*, 2600.

(4) Sung, S. Y.; Hsieh, C. L.; Law, A.; Zhau, H. E.; Pathak, S.; Multani, A. S.; Lim, S.; Coleman, I. M.; Wu, L. C.; Figg, W. D.; Dahut, W. L.; Nelson, P.; Lee, J. K.; Amin, M. B.; Lyles, R.; Johnstone, P. A.; Marshall, F. F.; Chung, L. W. *Cancer Res.* **2008**, *68*, 9996.

(5) Wu, J. B.; Shao, C.; Li, X.; Li, Q.; Hu, P.; Shi, C.; Li, Y.; Chen, Y. T.; Yin, F.; Liao, C. P.; Stiles, B. L.; Zhau, H. E.; Shih, J. C.; Chung, L. W. *J. Clin. Invest.* **2014**, *124*, 2891.

(6) True, L.; Coleman, I.; Hawley, S.; Huang, C. Y.; Gifford, D.; Coleman, R.; Beer, T. M.; Gelmann, E.; Datta, M.; Mostaghel, E.; Knudsen, B.; Lange, P.; Vessella, R.; Lin, D.; Hood, L.; Nelson, P. S. *Proc. Natl. Acad. Sci. U.S.A.* **2006**, *103*, 10991.

(7) Flamand, V.; Zhao, H.; Peehl, D. M. *J. Cancer Res. Clin. Oncol.* **2010**, *136*, 1761.

(8) Zhao, H.; Flamand, V.; Peehl, D. M. *BMC Med. Genomics* **2009**, *2*, 55.

(9) Siegel, R.; Ma, J.; Jemal, A. *CA Cancer J. Clin.* **2014**, *64*, 9−29.

(10) da Silva, F. C. *Curr. Opin. Urol.* **2011**, *21*, 248.

(11) Wilkins, A.; Parker, C. *Nat. Rev. Clin. Oncol.* **2010**, *7*, 583.

(12) Kapoor, D. A.; Zimberg, S. H.; Ohrin, L. M.; Underwood, W., 3rd; Olsson, C. A. *J. Urol.* **2011**, *186*, 860.

(13) Wang, G. L.; Jiang, B. H.; Rue, E. A.; Semenza, G. L. *Proc. Natl. Acad. Sci. U.S.A.* **1995**, *92*, 5510.

(14) Chandel, N. S.; Maltepe, E.; Goldwasser, E.; Mathieu, C. E.; Simon, M. C.; Schumacker, P. T. *Proc. Natl. Acad. Sci. U.S.A.* **1998**, *95*, 11715.

(15) Kaelin, W. G., Jr.; Ratcliffe, P. J. *Mol. Cell* **2008**, *30*, 393.

(16) Gerald, D.; Berra, E.; Frapart, Y. M.; Chan, D. A.; Giaccia, A. J.; Mansuy, D.; Pouyssegur, J.; Yaniv, M.; Mechta-Grigoriou, F. *Cell* **2004**, *118*, 781.

(17) Lu, X.; Kang, Y. *Clin. Cancer Res.* **2010**, *16*, 5928.

(18) De Colibus, L.; Li, M.; Binda, C.; Lustig, A.; Edmondson, D. E.; Mattevi, A. *Proc. Natl. Acad. Sci. U.S.A.* **2005**, *102*, 12684.

(19) Luo, S.; Zhang, E.; Su, Y.; Cheng, T.; Shi, C. *Biomaterials* **2011**, *32*, 7127.

(20) Tan, X.; Luo, S.; Wang, D.; Su, Y.; Cheng, T.; Shi, C. *Biomaterials* **2012**, *33*, 2230.

(21) Luo, S.; Tan, X.; Qi, Q.; Guo, Q.; Ran, X.; Zhang, L.; Zhang, E.; Liang, Y.; Weng, L.; Zheng, H.; Cheng, T.; Su, Y.; Shi, C. *Biomaterials* **2013**, *34*, 2244.

(22) Wu, J. B.; Shao, C.; Li, X.; Shi, C.; Li, Q.; Hu, P.; Chen, Y.-T.; Dou, X.; Sahu, D.; Li, W.; Harada, H.; Zhang, Y.; Wang, R.; Zhau, H. E.; Chung, L. W. K. *Biomaterials* **2014**, *35*, 8175.

(23) Yang, X.; Shi, C.; Tong, R.; Qian, W.; Zhau, H. E.; Wang, R.; Zhu, G.; Cheng, J.; Yang, V. W.; Cheng, T.; Henary, M.; Strekowski, L.; Chung, L. W. *Clin. Cancer Res.* **2010**, *16*, 2833.

(24) Gordon, R. R.; Wu, M. C.; Huang, C. Y.; Harris, W. P.; Sim, H. G.; Lucas, J. M.; Coleman, I.; Higano, C. S.; Gulati, R.; True, L. D.; Vessella, R.; Lange, P. H.; Garzotto, M.; Beer, T. M.; Nelson, P. S. *PLoS One* **2014**, *9*, e104271.

(25) Murphy, D. L.; Lipper, S.; Slater, S.; Shiling, D. *Psychopharmacology* **1979**, *62*, 129.

(26) Foraker, A. G. *Cancer* **1954**, *7*, 884.

(27) Thalmann, G. N.; Anezinis, P. E.; Chang, S. M.; Zhau, H. E.; Kim, E. E.; Hopwood, V. L.; Pathak, S.; von Eschenbach, A. C.; Chung, L. W. *Cancer Res.* **1994**, *54*, 2577.

(28) Tomayko, M. M.; Reynolds, C. P. *Cancer Chemother. Pharmacol.* **1989**, *24*, 148.

(29) Yang, X.; Shi, C.; Tong, R.; Qian, W.; Zhau, H. E.; Wang, R.; Zhu, G.; Cheng, J.; Yang, V. W.; Cheng, T.; Henary, M.; Strekowski, L.; Chung, L. W. *Clin. Cancer. Res.* **2010**, *16*, 2833.

(30) Zhau, H. E.; Odero-Marah, V.; Lue, H. W.; Nomura, T.; Wang, R.; Chu, G.; Liu, Z. R.; Zhou, B. P.; Huang, W. C.; Chung, L. W. *Clin. Exp. Metastasis* **2008**, *25*, 601.